Howard Hughes Medical Institute

Published as: *Nature*. ; 485(7399): 530–533.

Evolution of the Chalcone Isomerase Fold from Fatty Acid-Binding to Stereospecific Enzyme

Micheline N. Ngaki[1,*], **Gordon V. Louie**[2,*], **Ryan N. Philippe**[2,*], **Gerard Manning**[3], **Florence Pojer**[2], **Marianne E. Bowman**[2], **Ling Li**[1], **Elise Larsen**[2], **Eve Syrkin Wurtele**[1], and **Joseph P. Noel**[2]

[1]Department of Genetics, Development, and Cell Biology, Iowa State University, Ames, Iowa 50011, USA

[2]Howard Hughes Medical Institute, Jack H. Skirball Center for Chemical Biology and Proteomics

[3]Razavi Newman Center for Bioinformatics, The Salk Institute for Biological Studies, La Jolla, California 92037, USA

Abstract

Specialized metabolic enzymes biosynthesize chemicals of ecological importance, often sharing a pedigree with primary metabolic enzymes[1]. However, the lineage of the enzyme chalcone isomerase (CHI) remained a quandary. In vascular plants, CHI-catalyzed conversion of chalcones to chiral (*S*)-flavanones is a committed step in the production of plant flavonoids, compounds that contribute to attraction, defense[2], and development[3]. CHI operates near the diffusion limit with stereospecific control[4,5]. While associated primarily with plants, the CHI-fold occurs in several other eukaryotic lineages and in some bacteria. Here we report crystal structures, ligand-binding properties, and *in vivo* functional characterization of a non-catalytic CHI-fold family from plants. *A. thaliana* contains five actively transcribed *CHI-fold* genes, three of which additionally encode amino-terminal chloroplast-transit sequences (cTP). These three CHI-fold proteins localize to plastids, the site of *de novo* fatty acid (FA) biosynthesis in plant cells. Furthermore, their expression profiles correlate with those of core FA biosynthetic enzymes, with maximal expression occurring in seeds and coinciding with increased FA storage in the developing embryo.

Correspondence to: Eve Syrkin Wurtele[1] or Joseph P. Noel[2] Correspondence and requests for materials should be addressed to E.S.W. (mash@iastate.edu) or J.P.N. (noel@salk.edu.
*These authors contributed equally to this manuscript.

Supplementary Information is linked to the online version at www.nature.com/nature.

Author Contributions M.N.N. R.N.P., and G.V.L. made equivalent contributions and should be considered joint first authors. M.N.N. experimentally characterized the FAP genes *in planta*. M.E.B., R.N.P. and E.L. expressed, purified and crystallized proteins. L.L. designed genetics experiments and constructs. G.V.L. and F.P. carried out fatty acid binding analyses and solved the x-ray crystal structures. R.N.P. carried out thermal-shift assays of fatty acid binding. G.M. and E.L. performed phylogenetic and sequence analyses. J.P.N. designed the biochemical experiments; E.S.W. designed the bioinformatics and functional genomics experiments. The manuscript was written by R.N.P., G.V.L., M.N.N., J.P.N., G.M. and E.S.W.

Author Information Coordinates and structure factors have been deposited in the Protein Data Bank under accession codes 4DOI (AtCHI), 4DOK (AtCHIL), 4DOL (AtFAP3), and 4DOO (AtFAP1).

The authors declare no competing financial interests.

In vitro, these proteins are Fatty Acid-binding Proteins (FAP). FAP knockout *A. thaliana* plants exhibit elevated alpha-linolenic acid levels and marked reproductive defects, including aberrant seed formation. Notably, the FAP discovery defines the adaptive evolution of a stereospecific and catalytically 'perfected' enzyme[6] from a non-enzymatic ancestor over a defined period of plant evolution.

CHI (EC 5.5.1.6) catalyzes the intramolecular and stereospecific cyclization of chalcones to chiral flavanones via a Michael addition reaction[7]. The origin of CHI has been a mystery, due to the apparent absence of a related protein from primary metabolism[8]. CHI-like homologues in fungi and bacteria[9] lack both key catalytic residues and the chalcone-binding site of *bona fide* CHI (Fig. 1a-c, Supplementary Fig. 1). Phylogenetic analysis shows that CHI is restricted to vascular plants, and is derived from FAP3. FAP3 forms one of two branches of FAP proteins (FAP1 together with FAP2 form the other) found in derived and basal plants and is likely homologous to CHI-fold proteins from protists and fungi (Supplementary Figs. 2,3, Supplementary Files 1,2). *A. thaliana* has five genes (and one pseudogene not shown) encoding CHI-fold proteins: two CHI/CHI-like (CHIL) members, *AtCHI* (At3g55120) and *AtCHIL* (At5g05270), and three FAP members, *AtFAP1*, *AtFAP2* and *AtFAP3* (At3g63170, At2g26310, and At1g53520, respectively). Pairwise sequence identity of the shared CHI-fold domain ranges from 10% to 63%. AtCHI is a *bona fide* enzyme, and mutations of its gene result in plants devoid of flavonoids [10]. The active site of AtCHI retains residues important for catalytic activity, and AtCHI catalyzes the *in vitro* formation of (2*S*)-naringenin (Fig. 1c). In contrast, AtCHIL has substitutions of several catalytic residues (Supplementary Fig. 3). Likewise, *AtFAP1*, *AtFAP2* and *AtFAP3* encode substitutions at nearly all of the critical catalytic positions of AtCHI, and are devoid of catalytic activity (Supplementary Fig. 3). Studies with GFP fused to full-length FAP1, FAP2 and FAP3 indicate that these proteins localize in the plastid stroma (Supplementary Figs. 4a-d).

We determined X-ray crystal structures of AtCHI, AtCHIL, and the CHI-like domains of AtFAP1 and AtFAP3, and compared these to the previously reported structure of MsCHI[8]. Despite low sequence conservation, all structures align within 2.3 Åroot-mean-squared deviation for the backbone atoms of equivalent residues (Supplementary Fig. 5). Ligand-binding pockets reside within the helical layer, bounded by two α-helical segments (helix-turn-helix α6-α7 and helical hairpin α4-α5), β-hairpin β3a-β3b, and the face of the core β-sheet, β3a-β3f. Notably, the largest differences in backbone conformations of MsCHI, AtCHI and AtCHIL compared to AtFAP1 and AtFAP3 are confined to the secondary structure elements surrounding the ligand-binding pockets (Supplementary Fig. 5).

The most intriguing finding from the crystallographic structures is that the ligand-binding pockets of the recombinant FAP proteins are occupied by FAs (Fig. 2a-d). Clearly evident in electron-density maps are two abutting molecules of lauric acid (C12:0) in AtFAP1 (Fig. 2a, b), and one molecule of palmitic acid (C16:0) in AtFAP3 (Fig. 2c,d). The ligand-binding site of the FAP proteins encompasses a largely buried, non-polar cavity that sequesters the aliphatic chain(s) of the FAs, and a conserved Arg-Tyr pair that tethers a FA carboxylate group (Fig. 2b, d, and Supplementary Fig. 6). By comparison, CHI and CHIL possess more

sterically restricted pockets due to the presence of larger aliphatic residues and an inward shift of the secondary structure elements surrounding their ligand-binding clefts (Figs. 1, 2, and Supplementary Fig. 5). The CHI substrate-binding pocket also includes several polar residues that form key hydrogen-bond interactions with the chalcone substrate (in MsCHI, or with polar nitrate ions in AtCHI) (Fig. 1a, b). The corresponding residues in the FAPs are non-polar. AtCHIL possesses a distinct conservation pattern of the active site pocket (Supplementary Fig. 3). Extraction of ligands with ethanol followed by high performance liquid chromatography–mass spectrometry (HPLC-MS) analyses confirms that all three FAP proteins (including AtFAP2, which was recalcitrant to crystallization) associate with saturated FAs (Fig. 2e). In contrast, with AtCHI and AtCHIL produced under similar conditions, no associated FAs were detected analytically or crystallographically. Exogenous FAs were not supplied during FAP expression in *E. coli*, purification, or crystallization, so the ligands bound to the FAPs were likely acquired during expression and retained during purification to homogeneity. Indeed, these saturated FAs are among the most abundant FAs in *E. coli*[11].

There are indications that the true ligands of the FAPs *in planta* may be different FAs. In AtFAP1, the presence of two distinct non-polar tunnels, each occupied by the aliphatic chain of a C12:0 molecule (Fig. 2b and Supplementary Fig. 6a), may indicate a proclivity for longer chain FA recognition. In AtFAP3, the horseshoe-shaped conformation of C16:0 portends a preference for binding a *cis*-unsaturated C16 or C18 FA, which typically assumes a bent conformation (Fig. 2d and Supplementary Fig. 6b). Notably, AtFAP1 sequesters exogenously-supplied α-linolenic acid (C18:3), which presumably displaces the bound FAs acquired during expression in *E. coli* (Fig. 2e). We further assessed the binding by the FAPs of a series of common FAs using thermal-stability assays[12] (Supplementary Table 1). AtFAP3 interacts with most FAs tested and has maximal relative affinity for C16:0, though C18:0 induces greater thermal stabilization (Supplementary Fig. 7). AtFAP1 preferentially interacts with saturated FAs. However, the strongest stabilizing effect was observed with C18:3 (Supplementary Fig. 8), consistent with the displacement analyses (Fig. 2e) and perhaps a function of AtFAP1 in C18:3 metabolism as indicated also by phenotypic analysis. The thermal stability of AtCHI, included in these analyses as a negative control, was mostly unaffected by the addition of FAs (Supplementary Fig. 9).

We have obtained through a variety of approaches considerable direct and indirect evidence supporting the involvement of AtFAPs in FA metabolism. Network analysis of transcriptomic data[13,14] demonstrates maximal expression of *AtFAP1* and *AtFAP3* in seeds at six days after flowering (Supplementary Fig. 10a), coinciding with the accumulation of storage lipids in the developing embryo[15]. *AtFAP1* and *AtFAP3* co-express with genes encoding FA biosynthetic enzymes (Supplementary Fig. 10b). Developmental patterns of *AtFAP1*, *AtFAP2*, and *AtFAP3* expression were characterized in *A. thaliana* lines expressing a beta-glucuronidase (GUS) reporter under control of the respective promoters (Supplementary Figs. 11, 12, 13). The FAPs are highly expressed in developing cotyledons, young seedlings, roots, seeds, embryos, macrospores, preanthesis and tapetum. However, while *AtFAP2* is expressed throughout the life of the plant, expression of *AtFAP1* and especially *AtFAP3* is restricted to developing and reproductive tissues.

Homozygous *Atfap1* and *Atfap2* null plants were propagated from T-DNA insertion lines (Supplementary Figs. 14, 15). These *Atfap1* and *Atfap2* null plants are indistinguishable from wild-type (WT) plants during vegetative growth (Supplementary Figs. 17, 18), but the *Atfap1* mutants show marked differences during reproductive stages. Specifically, *Atfap1* siliques are shorter than those of wild type (∼18 mm *vs.* ∼20 mm) (Fig. 3a), mutant siliques contain 10-20% abnormal ovules (Fig. 3b), and the number of seeds per silique and the yield of viable seeds per plant are reduced in the *Atfap1* null lines (Fig. 3c). The *AtFAP3*-RNAi homozygote lines also present these phenotypic alterations. In addition, the vegetative phenotype of *AtFAP3*-RNAi is altered, demonstrating early bolting, fast growth, increased branching, reduced apical dominance and reduced overall plant height (Supplementary Fig. 19). No *AtFAP3*-RNAi line with more than a ∼50% reduction in *AtFAP3* RNA (relative to WT) could be identified, nor are any T-DNA tagged *Atfap3* knockout lines available. These data thus indicate that a functional *AtFAP3* is required for normal plant and embryo development. Double mutants bearing pairwise combinations of homozygous *Atfap1*, *Atfap2*, and *AtFAP3*-RNAi all show additive developmental effects (Supplementary Fig. 18).

Reciprocal crosses between WT and *Atfap1* or *AtFAP3*-RNAi lines point to the maternal inheritance of the aberrant reproductive phenotypes, as an elevated rate of ovule abortion is observed only in crosses in which the maternal parent is a null mutant (Supplementary Figs. 20-21, Supplementary Tables 2-7). The morphological phenotypes of >100 lines of heterozygotic *AtFAP3*-RNAi were analyzed; these consistently showed a restoration of the WT vegetative phenotype (Supplementary Fig. 22). However, the aberrant reproductive phenotype of the *AtFAP3*-RNAi mutant was maintained, indicating that phenotypic effects observed in the *AtFAP3*-RNAi lines are due to the specific knockdown of this gene. Analysis of FA composition reveals that *Atfap1* null lines have elevated total fatty-acid levels in both leaves and seeds relative to WT (Fig. 3d, e and g). These phenotypic alterations in leaves are temperature dependent (apparent only in plants grown at 15°C and 22°C) and due primarily to an increased level of the lower-melting-temperature unsaturated FA, C18:3. The FA content and distribution in leaves are indistinguishable between WT and mutant plants grown at 26°C (Fig. 3f). Similarly, *AtFAP3*-RNAi plants and *Atfap* double mutants have altered FA composition and increased FA content in leaves and seeds (Supplementary Fig. 23). This temperature-dependent phenotype reflects a decrease in the more fluid acyl chain component of trienoic FAs that accompanies increasing temperature[16,17].

We identified three relatives of CHI in *Arabidopsis* which appear to be FA-binding proteins of undetermined function. Phylogeny and sequence analyses indicate that the CHI fold occurs in most eukaryotic lineages (with the notable exception of animals) and even in bacteria. CHIL, as a divergent relative of FAP3, initially arose in mosses and may have served as the ancestor of enzymatic CHI in vascular plants (Supplementary Figs. 2 and 3). This ancestry for plant CHI clarifies the mystery surrounding the identity of the progenitor protein, and serves as a model to understand adaptation of a ligand-binding protein to a highly efficient and stereospecific enzyme. An evolutionary connection between fatty acid and flavonoid metabolism[18] is also evident from the structural and mechanistic similarities

between chalcone synthase (a type-III polyketide synthase (PKS)) acting one step upstream of CHI in the flavonoid pathway and ketoacyl-synthase III (KAS III) involved in chloroplast and bacterial fatty-acid biosynthesis. Together, CHI and CHS provide the foundation to examine the evolution of more recent metabolic pathways and metabolite classes from widespread biosynthetic pathways of primary metabolism.

Methods Summary

Structural biology

Crystal structures of the CHI domains of AtCHI, AtCHIL, AtFAP1, and AtFAP3 were determined as described in Supplementary Materials and Methods and summarized in Supplementary Table 8.

In vitro biochemistry

CHI activity was assayed[5,7]. Ligands bound to the purified AtFAP proteins were extracted with ethanol and analyzed by reversed-phase HPLC-MS. The effects of fatty acids (FAs) on the melting temperature of the AtFAP proteins were measured using a Thermofluor-based assay[12].

Phylogenetic and sequence analyses

Homologs of AtCHI were identified by iterative psi-blast and profile Hidden Markov Model (HMM). Alignments were curated using protein structure superpositions and homologous groups determined manually.

Informatics

Co-expression patterns of *A. thaliana* genes encoding FAP proteins and genes associated with FA biosynthesis were evaluated with data compiled from 72 microarray experiments using MetOmGraph (www.metnetdb.org)[13].

Plant growth and mutant analyses

Plants were grown in random block designs at 22°C under 16 hr light/8 hr dark. FAs were measured 5 hr after onset of light. Temperature effects were observed after 10-d growth at the specified temperatures. Homozygous *Atfap1-1, Atfap1-3, Atfap2-1* and *Atfap2*-2 mutant alleles (Supplementary Fig 14 and Supplementary Table 3) were generated from SALK_130560, SALK_039829, SAIL_171_C12 and SAIL_616_D09 (Arabidopsis Biological Resource Center, ABRC) stocks, respectively. *Atfap3* RNAi lines (Supplementary Fig. 16 and Supplementary Table 9) were generated from *A. thaliana* Col-0 plants, transformed with *Agrobacterium tumefasciens* strain GV3101 containing vector CATMA1a44560 (Nottingham Arabidopsis Stock Center, NASC)[19]. *AtFAP* RNA was quantified by RT-PCR (Supplementary Figs. 15 and 16). Transgenic *A. thaliana* lines were generated with *AtFAP1, 2, 3* promoters or promoter + cTP /or + CDS fused to GUS and green fluorescent protein (GFP).

FA quantification in plants

FAs were extracted from plant tissues using barium hydroxide hydrolysis[20], modified by methylation and analyzed by gas chromatography–mass spectrometry (GC-MS). Nonadecanoic acid was used as internal standard and a reference FA mixture was used for calibration and retention time determination (plantmetabolomics.org).

Supplementary Material

Refer to Web version on PubMed Central for supplementary material.

Acknowledgments

We thank A. Perera, B. Nikolau, H. Ilarsan and J. Peng for technical training (to M.N.N.), J. Peng for the *fap1-1* homozygote mutant line, D. Nettleton & H. Wang for statistical analysis of seed FA data, and Eric Scheeff for assistance in Bayesian phylogenetic analysis. This research was supported in part by a Fulbright Fellowship (M.N.N.). This material is based in part upon work supported by the National Science Foundation under Award No. MCB-0645794 (J.P.N.), EEC-0813570 (E.S.W.), MCB-0951170 (E.S.W.), and by the National Cancer Institute Award No. CA14195 (G.M.). J.P.N. is an investigator with the Howard Hughes Medical Institute. Portions of this research were conducted at the Advanced Light Source (ALS) a national user facility operated by Lawrence Berkeley National Laboratory, on behalf of the U.S. Department of Energy, Office of Basic Energy Sciences. The Berkeley Center for Structural Biology is supported in part by the Department of Energy, Office of Biological and Environmental Research, and by the National Institutes of Health, National Institute of General Medical Sciences. We thank the staff at the ALS for assistance with X-ray data collection. Any opinions, findings, and conclusions or recommendations expressed in this material are those of the author(s) and do not necessarily reflect the views of the National Science Foundation.

References

1. Hartmann T. From waste products to ecochemicals: fifty years research of plant secondary metabolism. Phytochem. 2007; 68:2831–2846.
2. Ferrer JL, Austin MB, Stewart C Jr, Noel JP. Structure and function of enzymes involved in the biosynthesis of phenylpropanoids. Plant Physiol Biochem. 2008; 46:356–370. [PubMed: 18272377]
3. Peer WA, Murphy AS. Flavonoids and auxin transport : modulators or regulators ? Trends Plant Sci. 2007; 21:556–563. [PubMed: 18198522]
4. Bednar RA, Hadcock JR. Purification and Characterization of Chalcone Isomerase from Soybeans. J Biol Chem. 1988; 263:9582–9588. [PubMed: 3384815]
5. Jez JM, Noel JP. Reaction mechanism of chalcone isomerase: pH dependence, diffusion control, and product binding differences. J Biol Chem. 2002; 277:1361–1369. [PubMed: 11698411]
6. Albery WJ, Knowles JR. Evolution of Enzyme Function and the Development of Catalytic Efficiency. Biochem. 1976; 15:5631–5640. [PubMed: 999839]
7. Jez JM, Bowman ME, Noel JP. Role of hydrogen bonds in the reaction mechanism of chalcone isomerase. Biochem. 2002; 41:5168–5176. [PubMed: 11955065]
8. Jez JM, Bowman ME, Dixon RA, Noel JP. Structure and mechanism of the evolutionarily unique plant enzyme chalcone isomerase. Nat Struct Biol. 2000; 7:786–791. [PubMed: 10966651]
9. Gensheimer M, Mushegian A. Chalcone isomerase family and fold: no longer unique to plants. Protein Sci. 2004; 13:540–544. [PubMed: 14718655]
10. Shirley BW, Hanley S, Goodman HM. Effects of ionizing radiation on a plant genome: analysis of two Arabidopsis transparent testa mutations. Plant Cell. 1992; 4:333–347. [PubMed: 1354004]
11. Oursel D, et al. Identification and relative quantification of fatty acids in *Escherichia coli* membranes by gas chromatography/mass spectrometry. Rapid Commun Mass Spectrom. 2007; 21:3229–3233. [PubMed: 17828792]
12. Niesen FH, Berglund H, Vedadi M. The use of differential scanning fluorimetry to detect ligand interactions that promote protein stability. Nat Protocols. 2007; 9:2212–2221. [PubMed: 17853878]

13. Mentzen WI, Wurtele ES. Regulon Organization of Arabidopsis. BMC Plant Biol. 2008; 8:99. [PubMed: 18826618]
14. Mentzen WI, Peng J, Ransom N, Nikolau BJ, Wurtele ES. Articulation of three core metabolic processes in Arabidopsis: fatty acid biosynthesis, leucine catabolism and starch metabolism. BMC Plant Biol. 2008; 8:76–90. [PubMed: 18616834]
15. Ruuska SA, Girke T, Benning C, Ohlrogge JB. Contrapuntal networks of gene expression during *Arabidopsis* seed filling. Plant Cell. 2002; 14:1191–1206. [PubMed: 12084821]
16. Falcone DL, Ogas JP, Somerville CR. Regulation of membrane fatty acid composition by temperature in mutants of Arabidopsis with alterations in membrane lipid composition. BMC Plant Biol. 2004; 4:17–31. [PubMed: 15377388]
17. Murakami Y, Tsuyama M, Kobayashi Y, Kodama H, Iba K. Trienoic fatty acids and plant tolerance of high temperature. Science. 2000; 287:476–479. [PubMed: 10642547]
18. Austin MB, Noel JP. The chalcone synthase superfamily of type III polyketide synthases. Nat Prod Rep. 2003; 20:79–110. [PubMed: 12636085]
19. Bonaventure G, Salas JJ, Pollard MR, Ohlrogge JB. Disruption of the *FATB* gene in *Arabidopsis* demonstrates an essential role of saturated fatty acids in plant growth. Plant Cell. 2003; 15:1020–1033. [PubMed: 12671095]
20. Hilson P, et al. Versatile gene-specific tags for *Arabidopsis* functional genomics: transcript profiling and reverse genetics applications. Gen Res. 2004; 14:2176–2189.
21. DeLano, WL. DeLano Scientific; San Carlos, CA, USA: 2002. The PyMOL Molecular Graphics System. http://www.pymol.org
22. Wallace AC, Laskowski RA, Thornton JM. LIGPLOT: A program to generate schematic diagrams of protein-ligand interactions. Prot Eng. 1995; 8:127–134.
23. Collaborative Computational Project Number 4. The CCP4 suite: programs for protein crystallography. Acta Crystallog. 1994; D50:760–763.

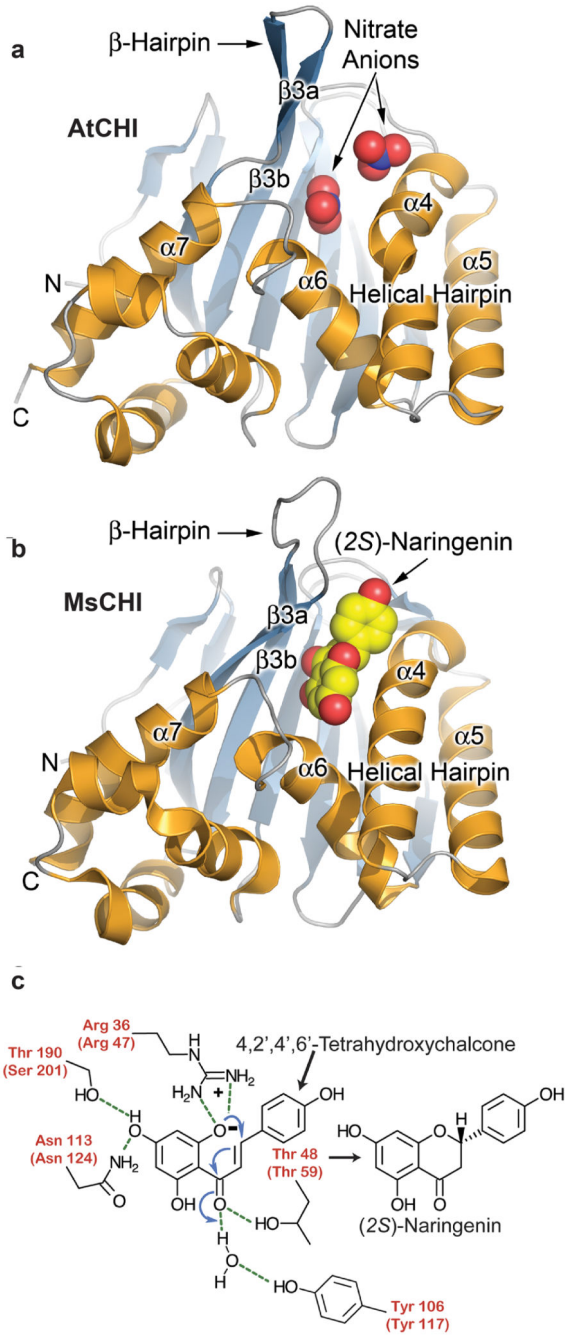

Figure 1. CHI fold, catalytic reaction and phylogeny

a, Ribbon diagram[21] of the AtCHI x-ray crystal structure, color-coded and labeled according to Jez *et al.*[8]. Two nitrate anions associate with catalytic residues in the substrate-binding site. **b**, Ribbon diagram[21] of the MsCHI structure bound to (2*S*)-naringenin[8]. **c**, Chalcone is converted to (2*S*)-flavanone (e.g. naringenin) using a combination of electrostatic catalysis and water-mediated charge stabilization during a stereospecific Michael-type addition reaction[5, 7-8]. Residue numbers for AtCHI appear in parentheses. Catalytic residues are colored red.

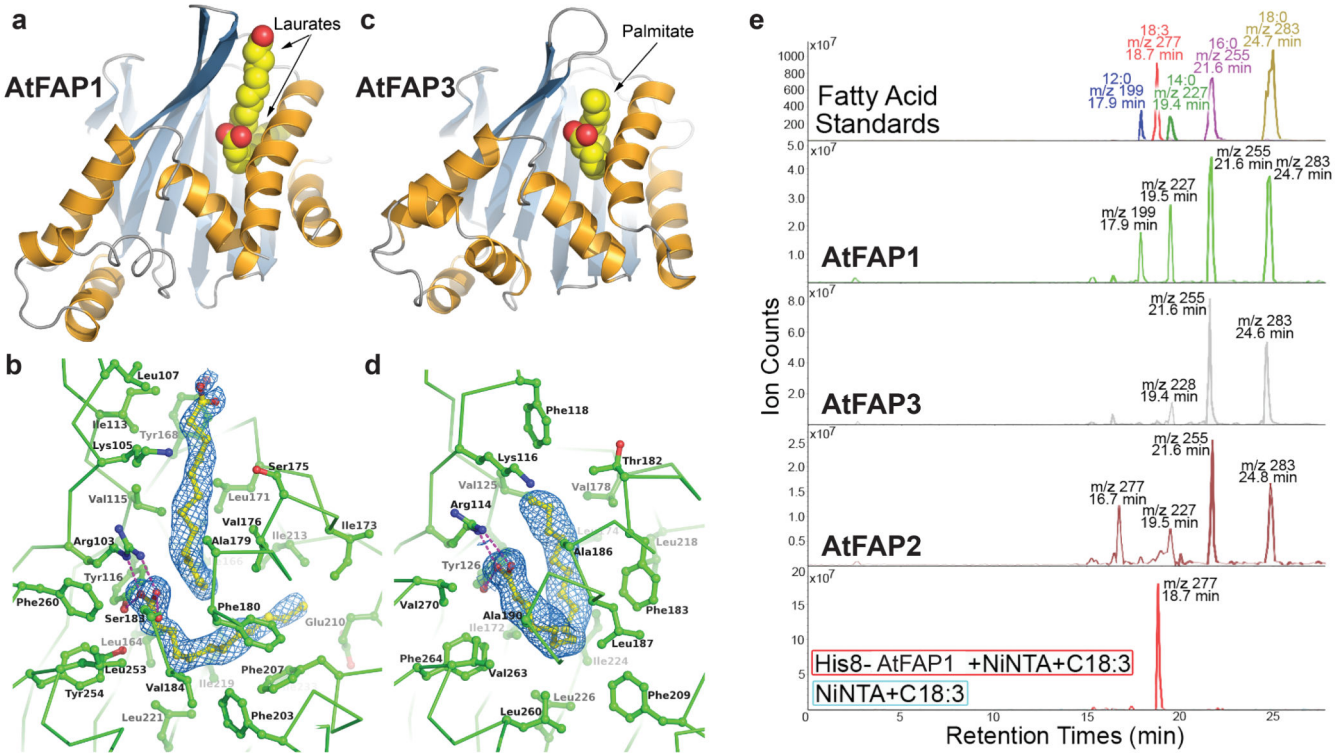

Figure 2. Three-dimensional structure and ligand binding of FAPs

a, Ribbon diagram[21] of AtFAP1 oriented and color-coded as in Fig. 1. The bound C12:0 molecules are shown as van der Waals spheres where carbon is yellow and oxygen is red. **b**, Close-up view of the AtFAP1 FA binding sites[21] with the experimental electron density of each C12:0 shown at 1σfor a SIGMAA-weighted 2Fo-Fc map[23]. **c**, Ribbon diagram[21] of AtFAP3 rendered as in **a. d**, Close-up view of the AtFAP3 FA binding site[21] with the C16:0 ligand shown as in **b. e**, Analysis of ligands associated with purified AtCHI-fold proteins separated and detected by reversed-phase HPLC-MS. The y-axes represent negative-ion counts for selected masses of anionic forms of FAs. The bottom panel depicts control (blue) and binding of C18:3 by His_8-tagged AtFAP1 (red) coupled to Ni-affinity resin.

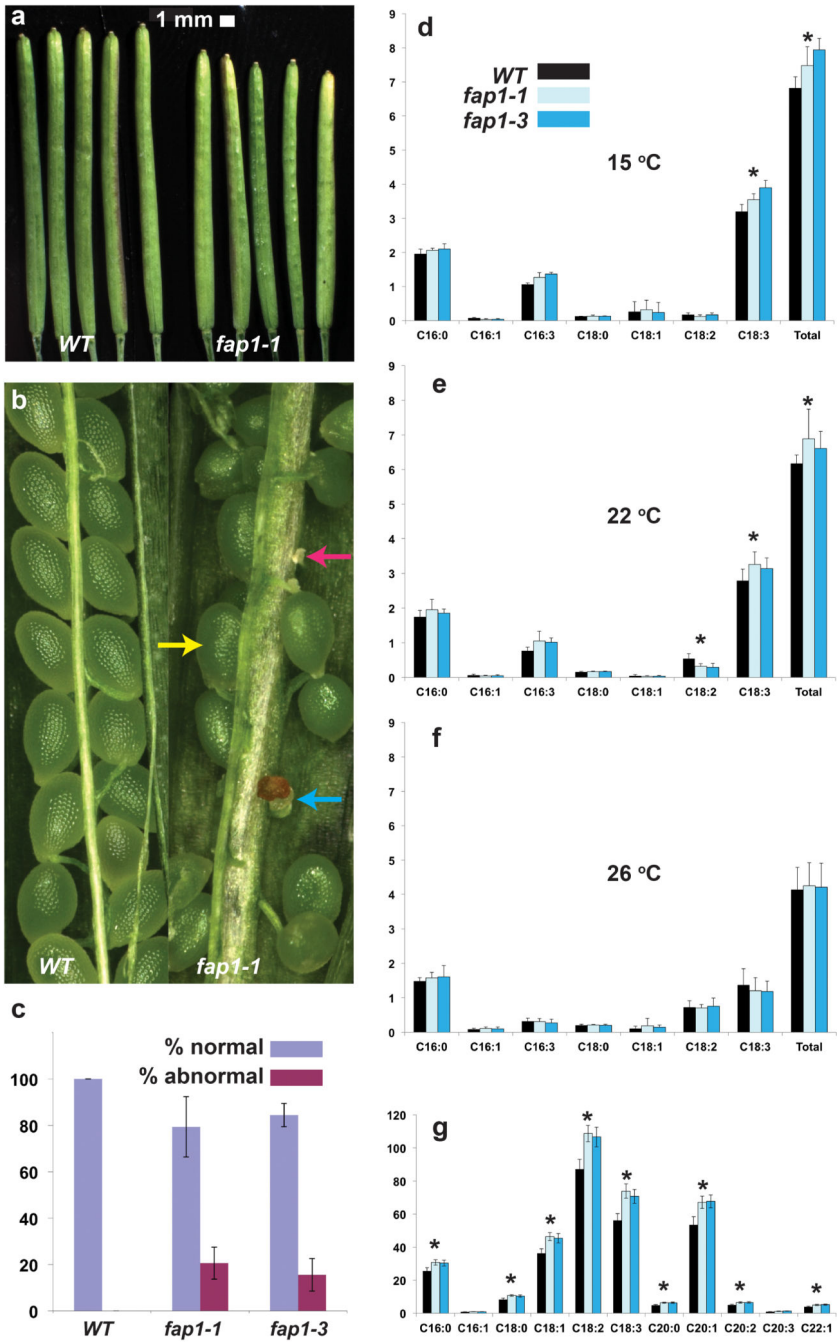

Figure 3. Phenotypic characterization of *Atfap1* null plants

a,Length of siliques 12 days after flowering; WT siliques are longer than siliques of *Atfap1* nulls (average length =17.8 mm for WT vs. 15.4 mm for *Atfap1-1*; 19.8 mm for WT vs. 17.1 mm for *Atfap1-3* (not shown); P <0.01, n=10 siliques/plant for 10 plants/genotype). **b**, *Atfap1* null siliques frequently contain abnormal ovules (normal, yellow arrow; aborted, blue arrow; unfertilized, pink arrow). **c**, *Atfap1* nulls have a greater percentage of abnormal (aborted and unfertilized) ovules than WT (P <0.01 and n=10 siliques/genotype) and low seed yield mass per plant (*Atfap1* average =1.3 g; WT average =1.5 g; P <0.01, n=10 plants).

FA content of leaves, y-axis=mg/g fresh weight, from plants grown at **d**, 15 °C; **e**, 22 °C; **f**, 26 °C. **d**, C18:3 and total FAs is greater in leaves of *Atfap1* nulls than WT. **e**, C18:3 and total FA is greater in leaves of *Atfap1* nulls than WT. **f**, *Atfap1* nulls and WT have similar FA content. **g**, In seeds of *Atfap1* mutants, C16:0, C18:0, C18:1, C18:2, C18:3, C20:0, C20:1, C20:2, C22:1, and total FAs (not shown) increase relative to WT. Asterisks (*, $P<0.05$) represent both *Atfap1* null lines; n=3 biological replicates, except for **g**, which has 3 experimental replicates with n=4 biological replicates; error bars represent standard deviation.